SANDIA REPORT
SAND2014-4877
Unlimited Release
Printed June 2014

Shadow Probability of Detection and False Alarm for Median-Filtered SAR Imagery

Ann Marie Raynal, John Miller, Edward Bishop, Volker Horndt, and Armin Doerry

Prepared by
Sandia National Laboratories
Albuquerque, New Mexico 87185 and Livermore, California 94550

Sandia National Laboratories is a multi-program laboratory managed and operated by Sandia Corporation,
a wholly owned subsidiary of Lockheed Martin Corporation, for the U.S. Department of Energy's
National Nuclear Security Administration under contract DE-AC04-94AL85000.

Approved for public release; further dissemination unlimited.

Issued by Sandia National Laboratories, operated for the United States Department of Energy by Sandia Corporation.

Printed in the United States of America. This report has been reproduced directly from the best available copy.

Available to DOE and DOE contractors from
U.S. Department of Energy
Office of Scientific and Technical Information
P.O. Box 62
Oak Ridge, TN 37831

Telephone:	(865) 576-8401
Facsimile:	(865) 576-5728
E-Mail:	reports@adonis.osti.gov
Online ordering:	http://www.osti.gov/bridge

Available to the public from
U.S. Department of Commerce
National Technical Information Service
5285 Port Royal Rd.
Springfield, VA 22161

Telephone:	(800) 553-6847
Facsimile:	(703) 605-6900
E-Mail:	orders@ntis.fedworld.gov
Online order:	http://www.ntis.gov/help/ordermethods.asp?loc=7-4-0#online

SAND2014-4877
Unlimited Release
Printed June 2014

Shadow Probability of Detection and False Alarm for Median-Filtered SAR Imagery

Ann Marie Raynal
ISR Analysis & Applications Department
Armin W. Doerry
ISR Mission Engineering Department
Sandia National Laboratories
P.O. Box 5800
Albuquerque, New Mexico 87185-MS0519

John Miller, Edward Bishop, and Volker Horndt
Mission Systems
General Atomics Aeronautical Systems, Inc.
San Diego, CA 92127

Abstract

Median filtering reduces speckle in synthetic aperture radar (SAR) imagery while preserving edges, at the expense of coarsening the resolution, by replacing the center pixel of a sliding window by the median value. For shadow detection, this approach helps distinguish shadows from clutter more easily, while preserving shadow shape delineations. However, the nonlinear operation alters the shadow and clutter distributions and statistics, which must be taken into consideration when computing probability of detection and false alarm metrics. Depending on system parameters, median filtering can improve probability of detection and false alarm by orders of magnitude. Herein, we examine shadow probability of detection and false alarm in a homogeneous, ideal clutter background after median filter post-processing. Some comments on multi-look processing effects with and without median filtering are also made.

ACKNOWLEDGEMENTS

This report was funded by General Atomics Aeronautical Systems, Inc. (ASI) Mission Systems.

General Atomics Aeronautical Systems, Inc. (GA-ASI), an affiliate of privately-held General Atomics, is a leading manufacturer of Remotely Piloted Aircraft (RPA) systems, radars, and electro-optic and related mission systems, including the Predator®/Gray Eagle®-series and Lynx® Multi-mode Radar.

CONTENTS

FIGURES

TABLES

NOMENCLATURE

dB	decibel
DOE	Department of Energy
MNR	Multiplicative Noise Ratio
NER	Noise Equivalent Reflectivity
PD	Probability of Detection
PFA	Probability of False Alarm
RMS	Root-Mean-Square
SAR	Synthetic Aperture Radar
SNL	Sandia National Laboratories

FOREWORD

This report details the results of an academic study. It does not presently exemplify any modes, methodologies, or techniques employed by any operational system known to the authors.

Classification

The specific mathematics and algorithms presented herein do not bear any release restrictions or distribution limitations.

The distribution limitations of this report are in accordance with the classification guidance detailed in the memorandum "Classification Guidance Recommendations for Sandia Radar Testbed Research and Development", DRAFT memorandum from Brett Remund (Deputy Director, RF Remote Sensing Systems, Electronic Systems Center) to Randy Bell (US Department of Energy, NA-22), February 23, 2004. Sandia has adopted this guidance where otherwise none has been given.

This report formalizes preexisting informal notes and other documentation on the subject matter herein.

1. INTRODUCTION

Algorithms for the detection of a target of interest in an image are generally concerned with the likelihood that the signal in an image is that of the target itself rather than background interference [1]. The calibrated radar reflectivity at a pixel, for point scatterers, or an area of pixels normalized by the resolution cell, for distributed scatterers, is assumed as the signal of the target or background interference, as appropriate. Target detection is a trade between the statistical likelihood that the target reflectivity is distinguishable from the interference (i.e. probability of detection or PD) and the likelihood that the interference reflectivity might be detected as the target (i.e. probability of false alarm or PFA). These probabilities are derived from the cumulative distributions of the expected target and interference signals up to a chosen threshold.

An occluded or dark region in synthetic aperture radar imagery, known as a shadow, is created when incident radar energy is obstructed by a target with height from illuminating resolution cells immediately behind the target in the ground plane. Shadow characteristics depend on the physical dimensions and mobility of a target, platform and radar imaging parameters, and scene clutter. Target shadow dimensions (e.g. length, area, or shape) and intensity can be important radar observables in SAR imagery for target detection, geolocation, and tracking, or even identification. Stationary target shadows can provide insight as to the physical dimensions of a target, while moving target shadows may show more accurately the location and motion of the target over time versus Doppler energy which may be shifted or smeared outside the scene. However, SAR shadows prove difficult to capture as a target or platform moves, since the quality of the no-return area may quickly be washed-out in a scene over many clutter resolution cells during an aperture. How distinct the intensity of a target shadow is from the intensity of interfering background clutter is crucial to shadow detection as a result.

The target one wants to distinguish, in the case of shadow detection, is noise against the interfering background clutter. The total noise in an image is the root-mean-square (RMS) sum of additive and multiplicative noise. Additive noise depends mostly on the ever-present thermal noise and radiometric emissions from the scene in the receiver electronics and adds to the image scene content. Multiplicative noise is proportional to the average scene intensity which can include clutter and point targets. That is,

$$\sigma_N = \sigma_n + \mathrm{MNR}\,\overline{\sigma_0}, \tag{1}$$

where σ_n is additive noise equivalent clutter reflectivity (NER); MNR stands for "multiplicative noise ratio" and is the aforementioned proportionality constant; and $\overline{\sigma_0}$ is the average scene backscatter. The computation of any normalized clutter reflectivity in an image (i.e. σ_n or σ_0) is the average of the pixel-to-pixel intensity fluctuations over the desired area [3], where intensity is defined as the power or magnitude squared pixel values of the image.

Shadow post-processing, detection, tracking, and identification algorithms may assist with target analysis, if the expectations on target shadow dimensions, intensity degradation, and desired radar and platform operating requirements are known. The reader is referred to the literature [2] for comprehensive details on the parameters that influence shadow intensity, as well as dimensions for generic targets. We merely state here for completeness in understanding that the ideal shadow length of a target will vary with the target height, target downrange depth, platform motion, platform grazing angle, and target motion. Increases in all but the latter two create longer and darker shadows. The ideal shadow width depends on the physical target width. Motion of a static target shadow during the formation of the synthetic aperture blurs the edges, widens the ideal width, and degrades the intensity (i.e. brightens) the shadow non-linearly with length, with the worst effects occurring toward the tip of the shadow farthest from the target. Larger frequencies, target widths, and resolutions, and shorter apertures, decrease these effects by diminishing the area span of the shadow and increasing the darkness of the shadow, while taller targets and higher grazing angles worsen it.

The shadow area of a moving target will be approximately a parallelogram while the target is in motion and will vary with the target's trajectory, relative to the platform. The shadow's swept area is minimized when the target moves only in range and decreases with increasing resolution, grazing angle, and platform velocity and decreasing range, target velocity, and target physical size due to shorter aperture times and smaller shadows. The intensity of a moving target shadow will be an average over the fraction of the time there is no return versus clutter return in a resolution cell during the synthetic aperture. For a target without a trajectory change during the aperture, the shadow intensity is related to the proportional clutter blockage (i.e. shadow area span) afforded by the target while in motion during the aperture versus the ideal static target physical shadow area. Target shadows are not expected to be visible for most cases where targets are mobile unless imaging parameters are carefully selected (e.g. shorter ranges, faster platforms, higher frequencies) to create quasi-static images of the target. Even so, the best achievable shadow differentiation from interfering background clutter will always be for a stationary target with small aperture motion.

The shadow region in a complex scene of multiple objects and clutter types is comprised of all possible object shadows, be they from the target of interest or not. Taller objects may block a desired target and its shadow return in a scene, making its characteristics unavailable for exploitation. For example a tall man-made structure or high-relief terrain feature may obscure the shadow of a target of interest. Furthermore, the shadow of a target of interest may be conglomerated with other object shadows or obfuscated by object scattering returns such as multipath or Doppler smear. Thus only if the shadow of a desired target is disjoint from all other object shadows and returns will its characteristics lend themselves pristinely for detection and target identification. This report assumes natural scenes where no interfering objects cast shadows or signals that might obfuscate the desired target shadow.

The probability distributions of a target and interference depend on the processing that is carried out for detection. Median filtering is a non-linear operation used to reduce speckle in SAR imagery while preserving edges. A sliding window of a chosen size replaces the image value at the center pixel of the window by the middle (i.e. median) value of the numerically sorted pixel values in the window. If the number of pixels in the window is even, the median value is usually taken as the average of the two middle values. Median filtering is useful for increasing the shadow-to-clutter ratio by the spatial filtering of the speckle of distributed targets in synthetic aperture radar imagery at the expense of resolution. The edge preserving nature of median filtering is beneficial for maintaining shadow shape definitions as well versus mean filtering. However, median filtering alters the statistical distributions of the target and interference reflectivities. Noise is assumed to be a complex, zero-mean, Gaussian random variable voltage, and thus a negative exponential distribution in intensity without filtering. Homogeneous, ideal clutter, σ_0, is Rayleigh distributed in amplitude and a negative exponential in intensity as well without filtering. After filtering, neither of these distributions holds. Herein, we consequently examine the effects of median filtering on shadow probability of detection and false alarm in SAR imagery for a homogeneous, ideal clutter background.

This report is organized as follows. Chapter 2 provides the general mathematical formulation of a distribution with median filtering. Chapter 3 builds on this knowledge to provide the distribution and statistical changes of median filtering to SAR imagery for homogeneous, fully-developed speckle. The chapter covers amplitude, intensity, and decibel power distribution effects. Chapter 4 summarizes a step-by-step procedure for computing probability of detection and false alarm, as well as provides example results with and without median filtering. Chapter 5 discusses the distributions, statistics, and effects of multi-looking, another common speckle reduction technique in SAR, in addition to median filtering. Conclusions are provided in Chapter 6.

"Truth is one forever absolute, but opinion is truth filtered through the moods, the blood, the disposition of the spectator."

- Wendell Phillips

2. GENERAL STATISTICS & DISTRIBUTIONS WITH MEDIAN FILTERING

The following general statistics and distributions apply for median filtering. Let the probability distribution that a pixel of an image takes on the value, X, be $p(X)$, [4, 5, 6]. X can be the image pixel amplitude, intensity, or decibel (dB) power value, though the distributions, $p(X)$, of each of these domains will be different.

The probability distribution of the sample median of an image for a filter window with N total pixels is then given by:

$$p_{Nmedian}(X) = f_N(y)p(X). \tag{2}$$

That is, the probability distribution of the sample median is the product of the probability of a pixel taking the value X times the probability that half the window samples are above or below the median intensity value of the image:

$$f_N(y) = \begin{cases} \frac{[y(1-y)]^{(N-1)/2}}{\beta\left(\frac{(N+1)}{2},\frac{(N+1)}{2}\right)} & ,for\ N\ odd \\ \frac{[y(1-y)]^{N/2}}{\beta\left(\frac{(N+2)}{2},\frac{(N+2)}{2}\right)} & ,for\ N\ even \end{cases}. \tag{3}$$

The variable y is the cumulative probability of the pixel values of the image, i.e.

$$y = P(y \leq X) = \int_{-\infty}^{X} p(y)dy. \tag{4}$$

β in Equation 3 is known in statistics as the "beta function" and represents the number of ways that half the samples above and below the window filter median can be arranged. The beta function is defined as:

$$\beta(a,b) = \frac{(a-1)!(b-1)!}{(a+b-1)!}, \tag{5}$$

which reduces in the particular cases of Equation 3 to:

$$\beta(a,a) = \frac{[(a-1)!]^2}{(2a-1)!} = \begin{cases} \frac{\left[\left(\frac{(N-1)}{2}\right)!\right]^2}{N!} & ,for\ N\ odd \\ \frac{\left[\left(\frac{N}{2}\right)!\right]^2}{(N+1)!} & ,for\ N\ even \end{cases}. \tag{6}$$

The general formulation for the probability distribution of the sample median from Equations 2 through 6 for an image pixel's value, $p(X)$, is then:

$$p_{Nmedian}(X) = \begin{cases} \frac{N!\left[P(y \le X)\left(1 - P(y \le X)\right)\right]^{\frac{(N-1)}{2}} p(X)}{\left[\left(\frac{(N-1)}{2}\right)!\right]^2} & , for\ N\ odd \\ \frac{(N+1)!\left[P(y \le X)\left(1 - P(y \le X)\right)\right]^{\frac{N}{2}} p(X)}{\left[\left(\frac{N}{2}\right)!\right]^2} & , for\ N\ even \end{cases} . \qquad (7)$$

The first- and second-order statistics of the probability distribution are given by:

$$\langle p_{Nmedian} \rangle = \int_{-\infty}^{\infty} X\, p_{Nmedian}\, dX, \text{ and} \qquad (8)$$

$$\sqrt{var(p_{Nmedian})} = \int_{-\infty}^{\infty} (X - \langle p_{Nmedian} \rangle)^2\, p_{Nmedian}\, dX. \qquad (9)$$

3. MEDIAN FILTERING FOR HOMOGENEOUS, FULLY-DEVELOPED SPECKLE SAR IMAGERY

The prior chapter laid the foundation regarding the general computation of distributions with median filtering. This chapter discusses image statistics, distributions, effects, and trends for median-filtered SAR imagery, specifically.

3.1. Image Statistics & Distributions

We base our analysis of median-filtered SAR image statistics and distributions on having homogeneous, fully-developed speckle. The fully-developed speckle property applies when [6, 7]:

1. the amplitude and phase of multiple elementary scatterers within a resolution cell are statistically independent quantities and independent between scatterers.
2. the number of scatterers is large and all scatterers are equally dominant in the resolution cell.
3. the scattering surface is dimensionally rough compared to the wavelength of the radar signal.

The above characteristics result in the multiplicative nature of speckle, where the j^{th} image intensity pixel can be defined as:

$$I(j) = R(j)S(j), \tag{10}$$

or the product of the uniformly distributed random processes of speckle-free ground reflectivity, R, times the speckle intensity, S.

For a single-look image of fully-developed speckle, the mean speckle intensity equals the standard deviation of the speckle intensity (which equal 1). I.e.,

$$\langle S \rangle = \sqrt{\mathrm{var}S} = 1. \tag{11}$$

In a single-look image, if a region is additionally homogeneous (i.e. uniform), the speckle-free ground reflectivity is a constant, R_0. The ratio of the second- to first-order statistics of the image, known as the coefficient of variation, is then equal to those of the speckle (which equal 1). I.e.,

$$\frac{\sqrt{\mathrm{varI}}}{\langle I \rangle} = \frac{R_0\sqrt{\mathrm{varS}}}{R_0\langle S \rangle} = \frac{\sqrt{\mathrm{varS}}}{\langle S \rangle} = 1. \tag{12}$$

In a single-look image, if the speckle-free ground reflectivity is otherwise textured (i.e. non-constant), more dominant or higher fluctuation pixels appear in a distributed target area. In this case, the coefficient of variation does not equal 1. I.e.,

$$\frac{\sqrt{\mathrm{varI}}}{\langle I\rangle} = \frac{\sqrt{\mathrm{varR}}\sqrt{\mathrm{varS}}}{\langle R\rangle\langle S\rangle} = \frac{\sqrt{\mathrm{varR}}}{\langle R\rangle} \neq 1. \tag{13}$$

The probability that a pixel of an image takes on the intensity value, I, for a homogeneous and textureless region of fully-developed speckle is the negative exponential distribution,

$$p(I) = \frac{1}{\langle I\rangle} e^{\left(-\frac{I}{\langle I\rangle}\right)}, \tag{14}$$

where $\langle I\rangle = \sqrt{\mathrm{var}I}$.

Furthermore, the probability that a pixel of an image takes on the amplitude value, A, for a homogeneous and textureless region of fully-developed speckle is the Rayleigh distribution,

$$p(A) = \frac{2A}{\langle I\rangle} e^{\left(-\frac{A^2}{\langle I\rangle}\right)}, \tag{15}$$

where $\langle I\rangle$ is as defined previously, and $A^2 = I$.

Lastly, the probability that a pixel of an image takes on the decibel value, D, for a homogeneous and textureless region of fully-developed speckle is:

$$p(D) = \frac{\ln 10}{10\langle I\rangle} e^{\left(\frac{D\ln 10}{10} - \frac{e^{\left(\frac{D\ln 10}{10}\right)}}{\langle I\rangle}\right)}, \tag{16}$$

where $\langle I\rangle$ is as defined previously, and $D = 10\log_{10} I$.

From Equation 4, it follows that the cumulative probability for the negative exponential intensity distribution is:

$$y = P(y \leq I) = 1 - e^{\left(-\frac{I}{\langle I\rangle}\right)}. \tag{17}$$

The cumulative probability for the Rayleigh amplitude distribution is:

$$y = P(y \leq A) = 1 - e^{\left(-\frac{A^2}{\langle I\rangle}\right)}. \tag{18}$$

The cumulative probability for the decibel power distribution is:

$$y = P(y \leq D) = 1 - e^{\left(-\frac{e^{\left(\frac{D\ln 10}{10}\right)}}{\langle I\rangle}\right)}. \tag{19}$$

Therefore, the probability distributions of the sample median for a homogeneous, textureless region of fully developed speckle in a single-look image (by substituting respective $p(X)$ and

$P(y \leq X)$ from Equations 14 through 16 and Equations 17 through 19 into Equation 7) are as follows for intensity, amplitude, and decibel power, respectively:

$$p_{Nmedian}(I) = \begin{cases} \dfrac{N!\left[e^{\left(-\frac{I}{\langle I \rangle}\right)}\right]^{(N+1)/2}\left[1-e^{\left(-\frac{I}{\langle I \rangle}\right)}\right]^{(N-1)/2}}{\langle I \rangle\left[\left(\frac{(N-1)}{2}\right)!\right]^2}, & for\ N\ odd \\ \dfrac{(N+1)!\left[e^{\left(-\frac{I}{\langle I \rangle}\right)}\right]^{(N+2)/2}\left[1-e^{\left(-\frac{I}{\langle I \rangle}\right)}\right]^{N/2}}{\langle I \rangle\left[\left(\frac{N}{2}\right)!\right]^2}, & for\ N\ even \end{cases}, \qquad (20)$$

$$p_{Nmedian}(A) = \begin{cases} \dfrac{2AN!\left[e^{\left(-\frac{A^2}{\langle I \rangle}\right)}\right]^{(N+1)/2}\left[1-e^{\left(-\frac{A^2}{\langle I \rangle}\right)}\right]^{(N-1)/2}}{\langle I \rangle\left[\left(\frac{(N-1)}{2}\right)!\right]^2}, & for\ N\ odd \\ \dfrac{2A(N+1)!\left[e^{\left(-\frac{A^2}{\langle I \rangle}\right)}\right]^{(N+2)/2}\left[1-e^{\left(-\frac{A^2}{\langle I \rangle}\right)}\right]^{N/2}}{\langle I \rangle\left[\left(\frac{N}{2}\right)!\right]^2}, & for\ N\ even \end{cases}, \text{ and} \qquad (21)$$

$$p_{Nmedian}(D) = \begin{cases} \dfrac{e^{\left(\frac{D\ln 10}{10}\right)}\ln 10 N!\left[e^{\left(-\frac{e^{\left(\frac{D\ln 10}{10}\right)}}{\langle I \rangle}\right)}\right]^{(N+1)/2}\left[1-e^{\left(-\frac{e^{\left(\frac{D\ln 10}{10}\right)}}{\langle I \rangle}\right)}\right]^{(N-1)/2}}{\langle I \rangle\left[\left(\frac{(N-1)}{2}\right)!\right]^2}, & for\ N\ odd \\ \dfrac{e^{\left(\frac{D\ln 10}{10}\right)}\ln 10(N+1)!\left[e^{\left(-\frac{e^{\left(\frac{D\ln 10}{10}\right)}}{\langle I \rangle}\right)}\right]^{(N+2)/2}\left[1-e^{\left(-\frac{e^{\left(\frac{D\ln 10}{10}\right)}}{\langle I \rangle}\right)}\right]^{N/2}}{10\langle I \rangle\left[\left(\frac{N}{2}\right)!\right]^2}, & for\ N\ even \end{cases}. \qquad (22)$$

Equations 20 through 22 are cumbersome, and so the solution to Equation 7 is often found numerically. The cumulative probability distributions found from applying Equation 4 to these median filtered distributions provide the PD and PFA after filtering.

3.2. Effects and Trends of Filtering

Suppose that we have a region of homogeneous, textureless, fully-developed speckle where $\langle I \rangle = \sqrt{\text{var}I} = 1$ and use a $\sqrt{N}$x$\sqrt{N}$ median filter on the image region. The effects and trends of median filtering on the image as a function of $N$are as follows.

Figure 1 shows the difference in the probability distribution and statistics of the intensity image region, $p(I)$, versus the median-filtered image region, $p_{Nmedian}(I)$. The mean and standard deviation of the intensity decrease by 1.27 dB and 4.67 dB, respectively, for a 3x3 window. The statistics further decrease with increasing filter window size. Furthermore, the median-filtered distributions approach a Gaussian with increasing window size. These general trends are true irrespective of the domain in which median filtering occurs, as can be observed in Figure 2 and Figure 3 for amplitude and decibel power as well. (N.b. The square root of the mean intensity, median filtered or otherwise, is not equal to the mean of the amplitude distribution, median filtered or otherwise. This assumption is a common pitfall.) Per [4], the mean and standard deviations of median filtered images approach the values in Table 1 as N becomes large. In short, when formulating PD and PFA models for imagery where median filtering has been applied, the models need to include filter statistical biases of the pixel value probability distributions.

Table 1. Asymptotic Values of the Mean and Standard Deviation of a Median Filtered Homogeneous, Ideal Clutter Area for Large N

	Mean	Standard Deviation
Intensity	$\langle I \rangle \ln 2$	$\langle I \rangle / \sqrt{N}$
Amplitude	$\sqrt{\langle I \rangle \ln 2}$	$0.6\sqrt{\langle I \rangle / N}$
Decibel Power (dB)	$10\log_{10}\langle I \rangle - 1.59$	$6.3/\sqrt{N}$

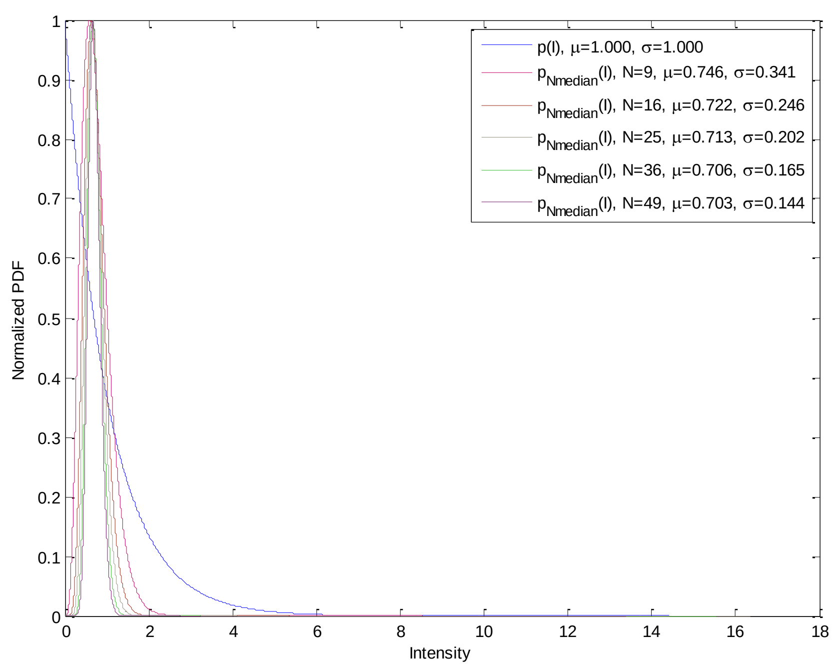

Figure 1. Probability Distribution & Statistics of Image Intensity with Ideal Speckle and Corresponding Median-Filtered Intensity for Varying Window Pixels, N

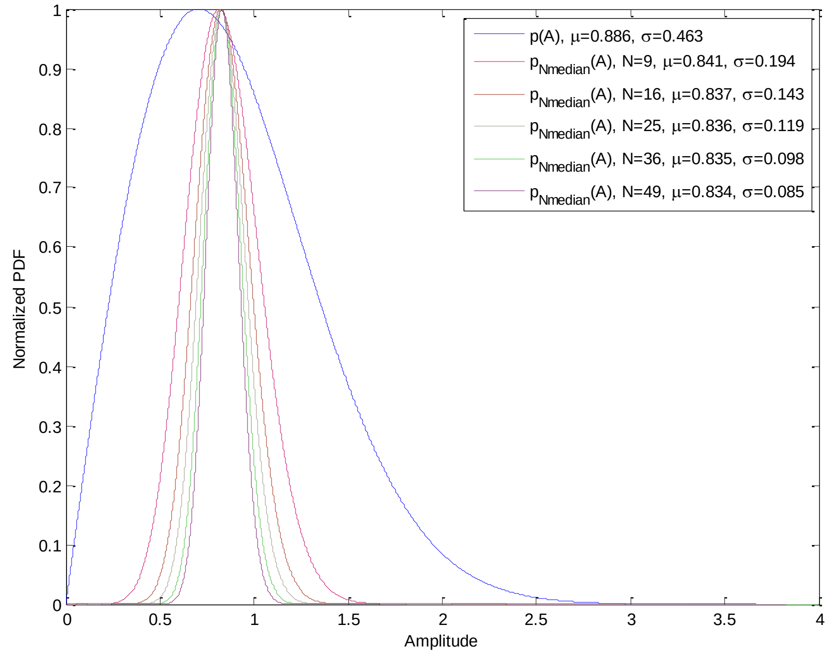

Figure 2. Probability Distribution & Statistics of Image Amplitude with Ideal Speckle and Corresponding Median-Filtered Amplitude for Varying Window Pixels, *N*

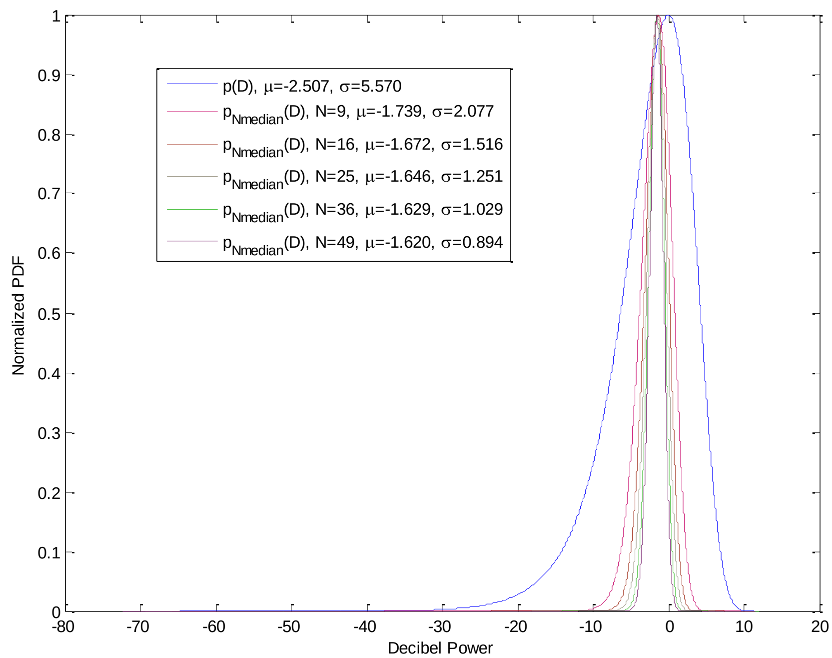

Figure 3. Probability Distribution & Statistics of Image in Decibels with Ideal Speckle and Corresponding Decibel Median-Filtered Image for Varying Window Pixels, *N*

"Our eyes only see the big dimensions, but beyond those there are others that escape detection because they are so small."

- Brian Greene

4. SHADOW PD AND PFA FOR MEDIAN-FILTERED IMAGERY

Prior chapters have examined the mathematical framework for median filter post-processing effects on SAR imagery. This chapter leverages those results to compute the shadow probability of detection and false alarm in SAR imagery. A methodology and an example are given.

4.1. Methodology

In order to compute the probability of detection and probability of false alarm of a shadow amidst background clutter with median filtering, we must do the following:

1. Determine the noise equivalent clutter reflectivity of the radar,
2. Determine the multiplicative noise ratio of the radar,
3. Establish a clutter background intensity,
4. Compute the average total noise from Equation 1,
5. Compute the median filtered probability distributions of total noise and the clutter background from Equation 7 numerically, or analytically by using the results of Equations 20 through 22, for the desired image domain and window size,
6. Find the cumulative distribution up to a given threshold from the total noise distribution in step 6 as the PD, and
7. Find the cumulative distribution up to a given threshold from the clutter distribution in step 6 as the PFA.

For simplicity, we make the assumption that the homogeneous, ideal background clutter surrounding a shadow area is the same as the average scene intensity value for the computation of multiplicative noise in step 4. Generally, a scene will contain many types of clutter (where $\overline{\sigma_0} \neq \sigma_0$), thus increasing the multiplicative noise. We further emphasize that the shadows of moving targets will blur the shadow with clutter over the synthetic aperture, additionally decreasing the discrimination between the shadow and clutter [2]. Therefore, the static target PD and PFA give the best case results one might expect for a target. Finally, note that this process is general for determining PD and PFA without median filtering if in step 5, Equations 14 through 16 replace the current procedure, or step 5 is foregone altogether and Equations 17 through 19 are leveraged for step 6 and 7 directly.

4.2. Example Computation

We now proceed to illustrate the computation of PD and PFA based on the provided methodology.

1. A basic equation for the noise equivalent radar reflectivity of a SAR system is [8]:

$$\sigma_n = \frac{256\pi^3 kT}{c}\left(R^3 v_x \cos\psi_g\right)\left(\frac{B_T F_N L_{radar} L_{atmos}}{P_{avg} {G_A}^2 \lambda^3}\right)\left(\frac{L_r L_a}{a_{wr} a_{wa}}\right), \tag{23}$$

where we assume the parameter definitions of Table 2. Most radar systems are capable of many ranges, velocities, and grazing angles. However, the worst case NER will be given by the longest ranges, lowest grazing angles, and fastest platform velocities. For illustrative purposes, we select the values noted, which provide the NER in the table.

Table 2. Noise Equivalent Clutter Reflectivity Parameter Assumptions

Parameter	Symbol	Units	Value
Boltzmann's constant	k	J/K	1.38 x 10^{-23}
Standard temperature	T	K	290
Speed of light	c	m/s	3 x 10^8
Noise figure	F_N	dB	4
Radar losses	L_{radar}	dB	2
Antenna gain	G_A	dBi	30
Range losses	L_r	dB	1
Azimuth losses	L_a	dB	1
Range Window Factor	a_{wr}	-	1.1822
Azimuth Window Factor	a_{wa}	-	1.1822
Average Power	P_{avg}	W	100
Wavelength	λ	m	0.02 m
Bandwidth at 4" Range Resolution	B_T	Hz	1.75 x 10^9
Range	R	m	{5000, 10000, 20000}
Atmospheric losses	L_{atmos}	dB	0.00005R = {0.25,0.5,1}
Platform Velocity	v_x	m/s	100
Grazing Angle	ψ_g	°	10
Step 1: Noise Equivalent Reflectivity	$\boldsymbol{\sigma_n}$	**dB**	**{-48.7, -39.4, -29.9} @ 5, 10, 20 km range**
Step 2: Multiplicative Noise Ratio	**MNR**	**dB**	**-18.2**
Step 3: Background Clutter Reflectivity	$\boldsymbol{\sigma_0}$	**dB**	**{-24.5 (asphalt), -16.5 (soil)}**
Multiplicative Noise	MNR $\overline{\sigma_0}$	dB	{-42.7 (asphalt), -34.7 (soil)}
Step 4: Total Noise	$\boldsymbol{\sigma_N}$	**dB**	**{-41.7, -37.7, -29.6 (asphalt); -34.5, -33.4, -28.6 (soil)} @ 5, 10, 20 km range**

2. We assume an MNR of -18.2 dB, which is reasonable for many SAR systems [3, 9].

3. At the chosen grazing angle and frequency, the worst case (minimum) clutter reflectivity of dry asphalt is -24.5 dB and dry soil is -16.5 dB per Figure 4, which are reasonable clutter types against which one might want to detect moving target shadows.

4. The expected multiplicative noise and total noise for asphalt and soil, respectively, is provided in Table 2 for the assumed ranges as appropriate. At the shorter ranges, multiplicative noise dominates total noise, but at longer ranges, additive noise dominates the total noise.

5. Figure 5, Figure 6, and Figure 7 show the shadow and clutter distributions before and after 5x5 median filtering as a function of range for dry asphalt and soil for the amplitude, intensity, and decibel power domains. The median filtering causes the shadow and clutter distributions to narrow, look more Gaussian-like, and increase in

separation, as expected. In addition, the separation between shadow and clutter distributions is greater for shorter ranges due to decreased total noise levels, irrespective of filtering. Lastly, note that the separation between shadow and clutter for asphalt is far less than that of soil, particularly at longer ranges where the total noise levels approach those of the asphalt.

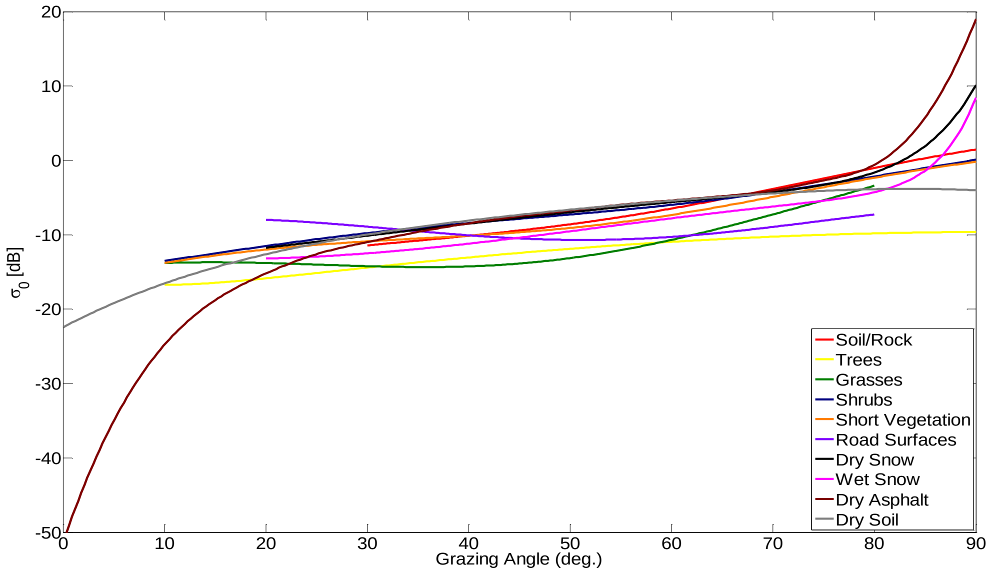

Figure 4. Mean Clutter Reflectivities as a Function of Type and Grazing Angle [10]

6. Figure 8 shows the probability of detection of a shadow versus the threshold that yields such a PD for each image domain before and after 5x5 median filtering as a function of range and clutter type. For a given threshold value, the PD is generally greater with median filtering than without for high PD values. Furthermore, the thresholds to achieve the same PD at longer ranges are much higher than at shorter ranges.

7. Figure 9 shows the probability of false alarm versus the threshold that yields such a PFA as a function of range and clutter type before and after 5x5 median filtering. From Figure 8 and Figure 9 we derive Figure 10, which shows the probability of detection versus false alarm. The PFA is generally far greater without filtering than with filtering. We further observe that the PFA is orders of magnitude worse, despite filtering, for the long-range cases where total noise approaches the clutter levels (particularly for asphalt). Finally, we observe that PFA values no better than about 10^{-15} should be expected for high PD values when worst case platform and imaging parameters apply for a static target. Moving target shadows will further worsen the PFA and PD. Slower platforms and higher grazing angles may improve the PFA and PD due to lower total noise values and higher clutter values. (These measures only help to a degree, however. Slower platforms also lengthen the synthetic aperture which causes more shadow blurring with clutter, particularly for moving targets. Higher grazing angles also shorten the shadow length, decreasing the available shadow area for detection.)

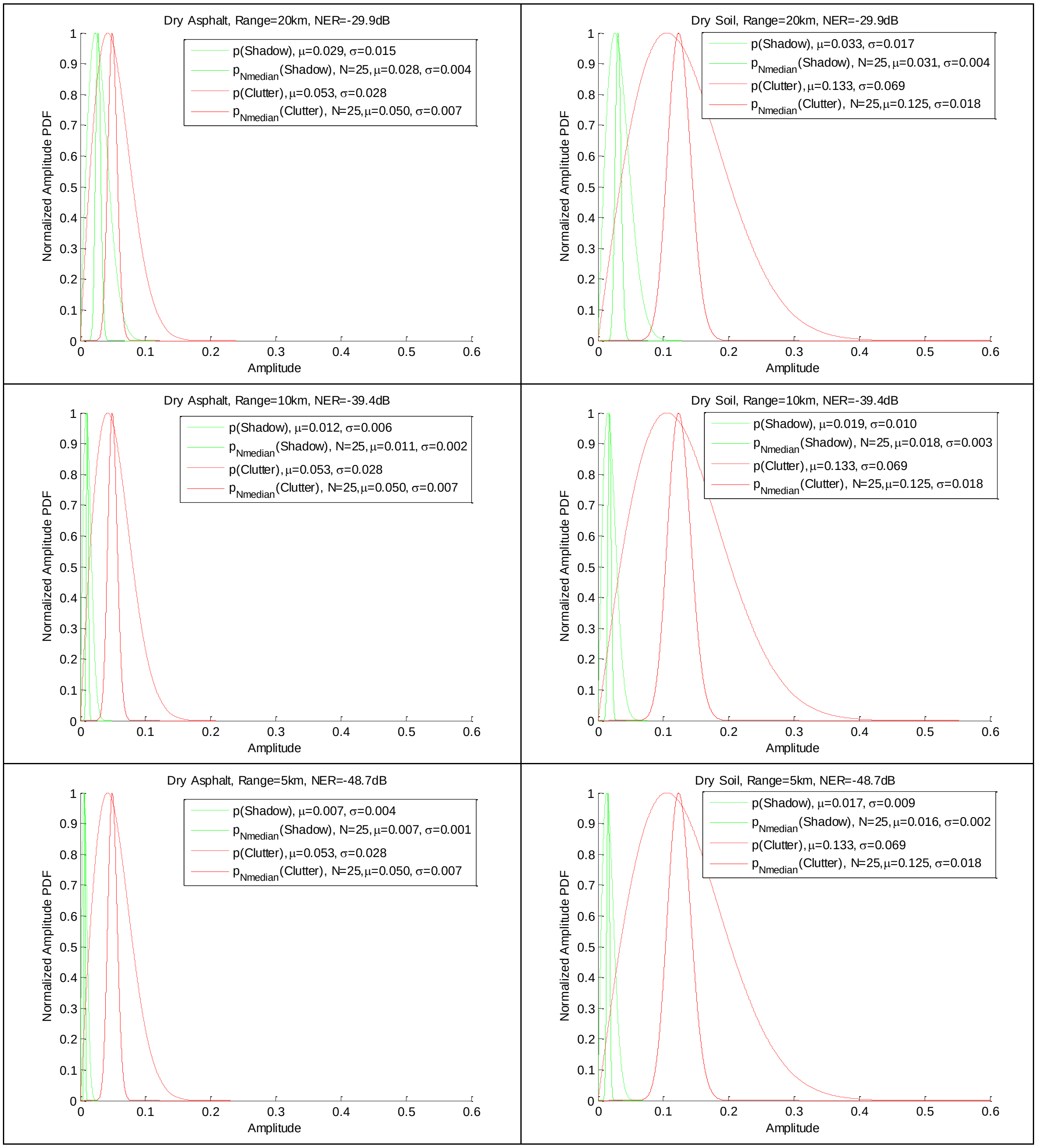

Figure 5. Step 5: Amplitude Distributions of Shadow and Clutter Before and After 5x5 Median Filtering for Asphalt and Soil versus Range

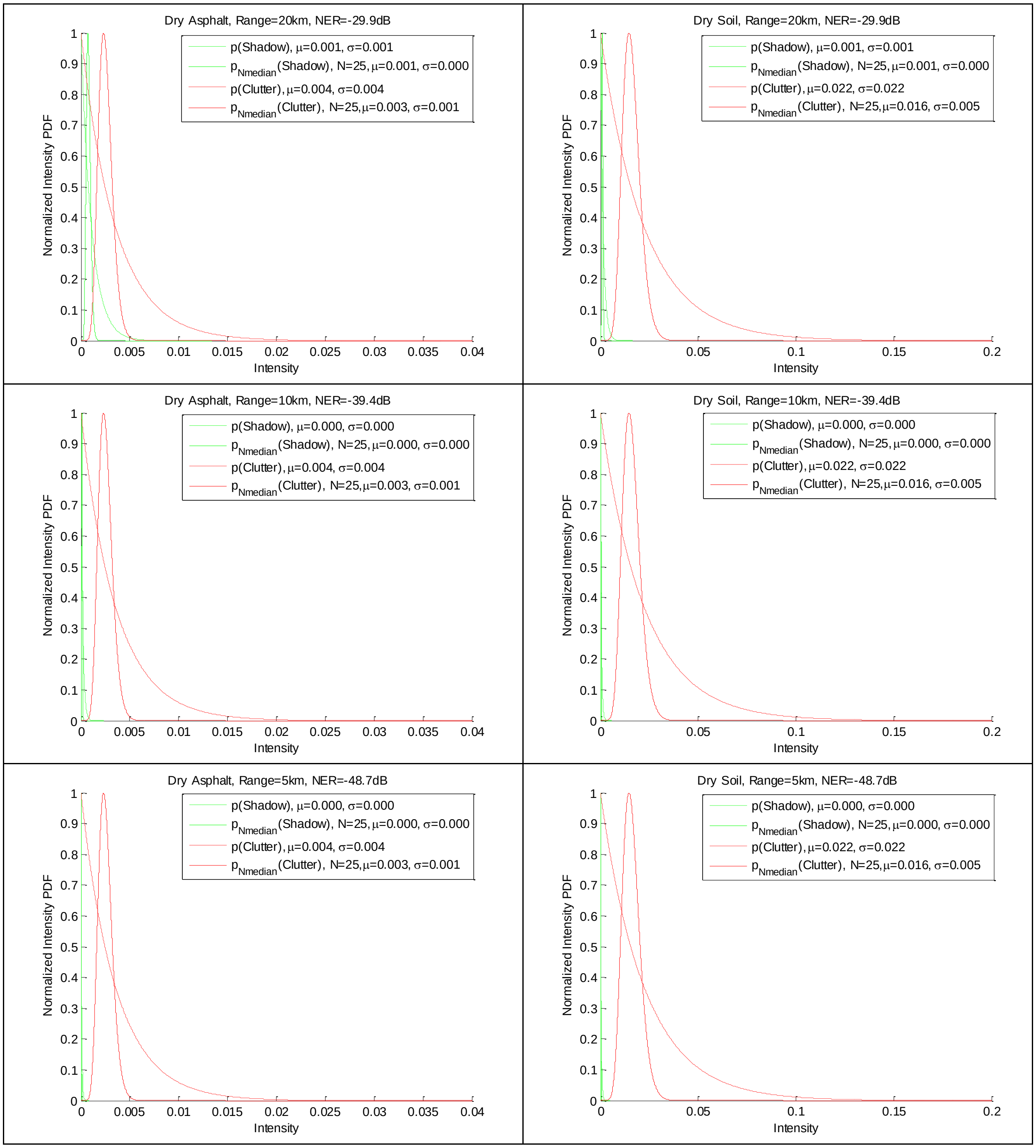

Figure 6. Step 5: Intensity Distributions of Shadow and Clutter Before and After 5x5 Median Filtering for Asphalt and Soil versus Range

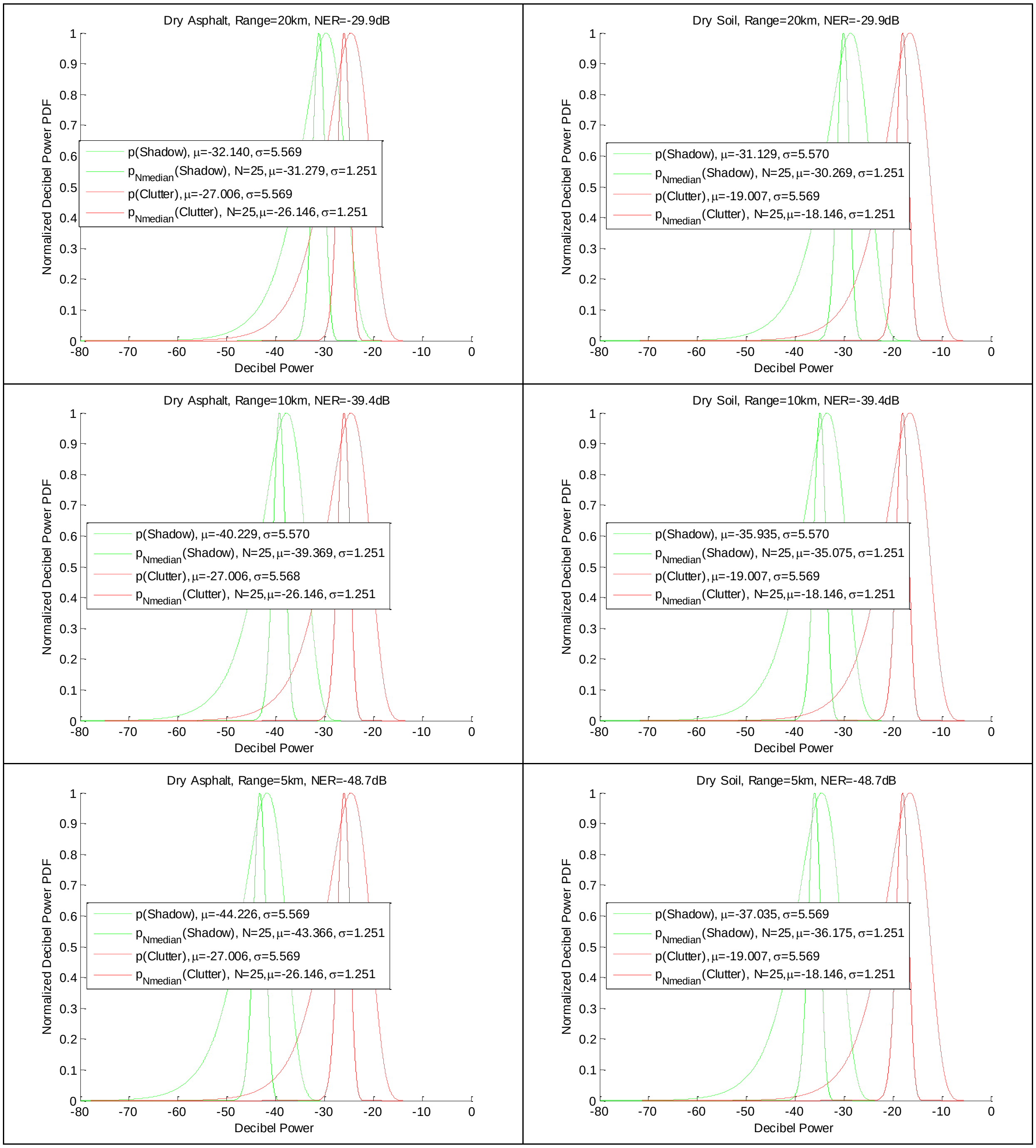

Figure 7. Step 5: Decibel Power Distributions of Shadow and Clutter Before and After 5x5 Median Filtering for Asphalt and Soil versus Range

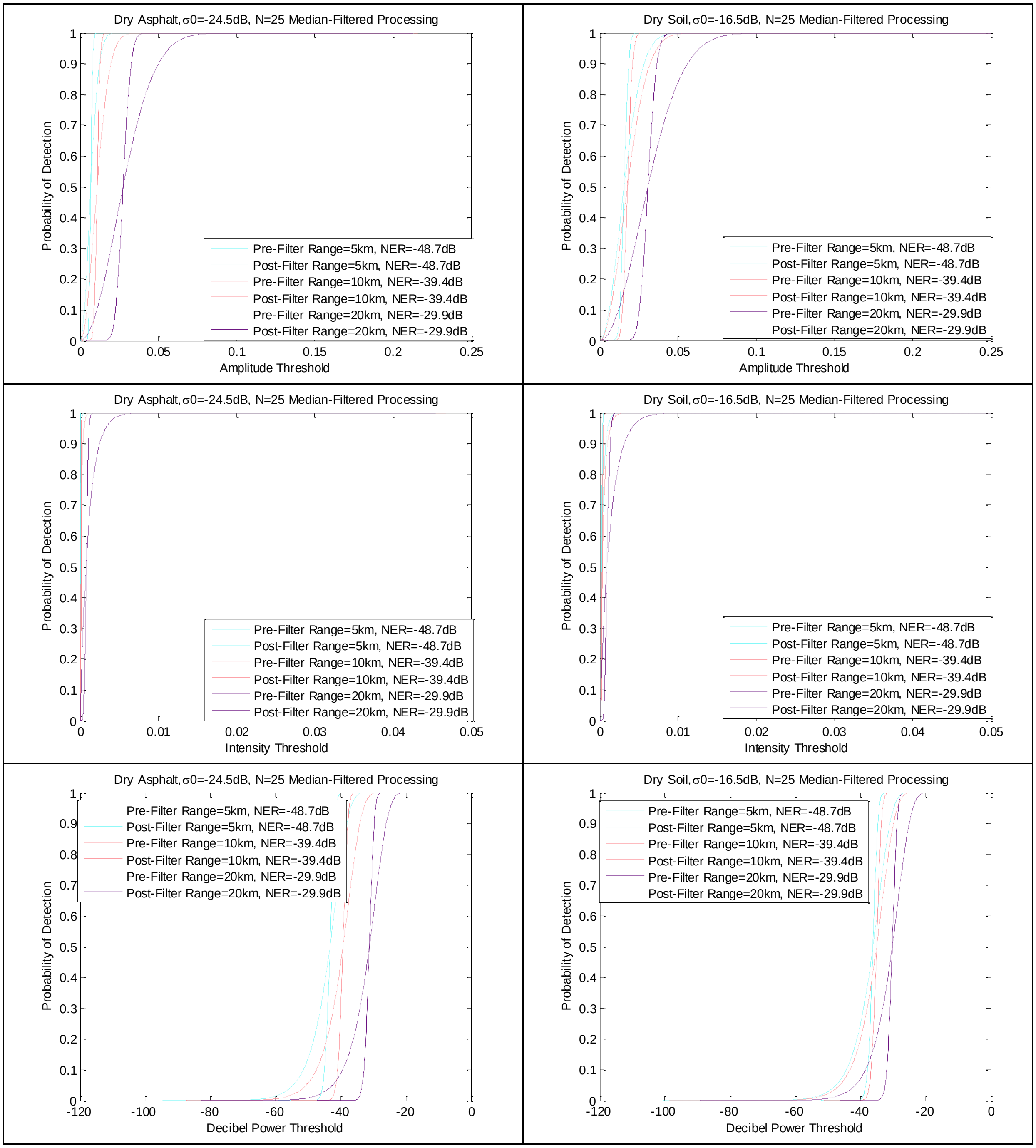

Figure 8. Step 6: Thresholds for PD Before and After 5x5 Median Filtering for Asphalt and Soil versus Range

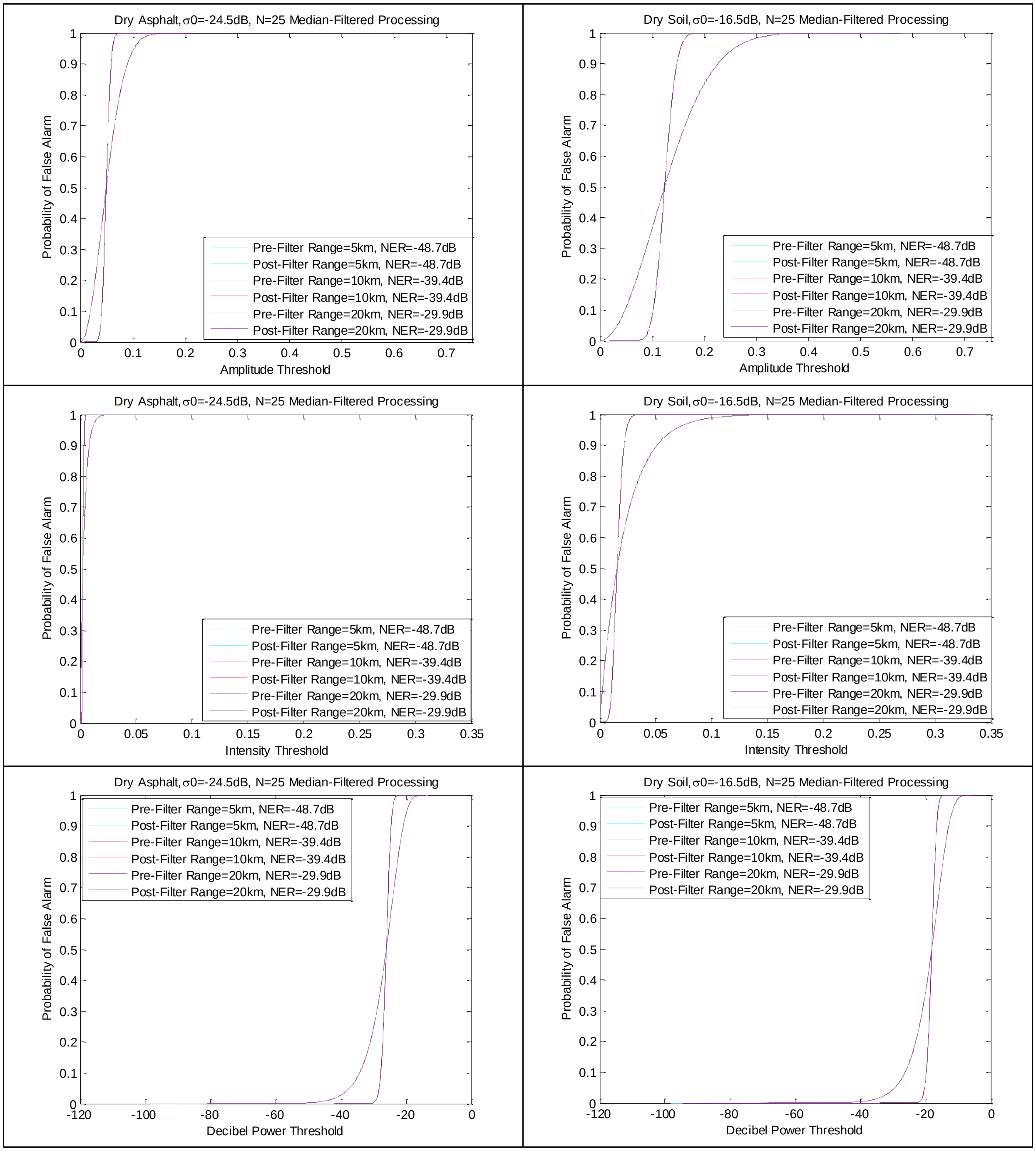

Figure 9. Step 7: Thresholds for PFA Before and After 5x5 Median Filtering for Asphalt and Soil versus Range

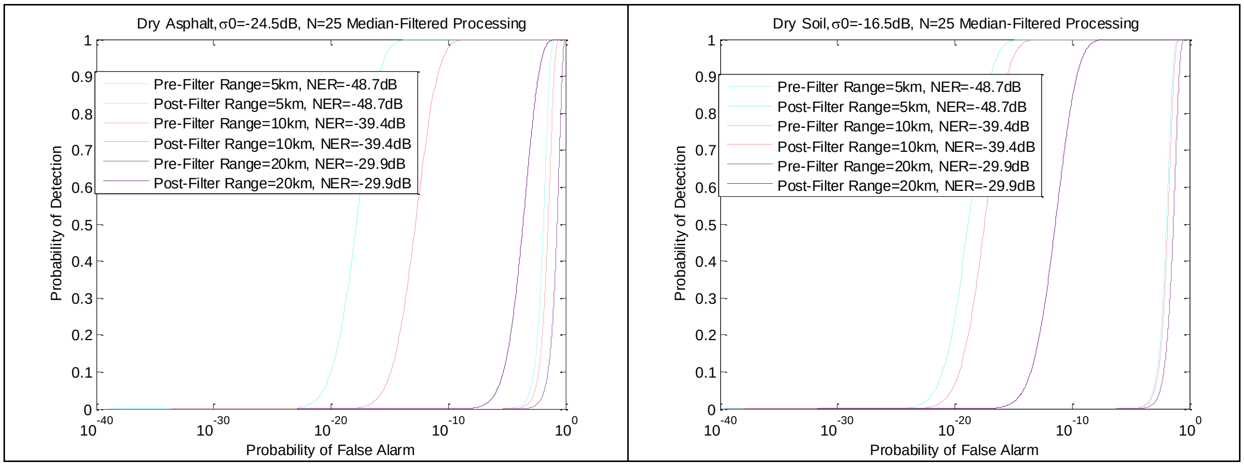

Figure 10. Step 6 and 7: PD and PFA Before and After 5x5 Median Filtering for Asphalt and Soil versus Range

"The past is not simply the past, but a prism through which the subject filters his own changing self-image."

- Doris Kearns Goodwin

5. SHADOW PD AND PFA FOR MULTI-LOOKED & MEDIAN-FILTERED IMAGERY

Multi-look processing (i.e. the incoherent averaging of many intensity images of the same scene) also impacts the statistical properties of shadows and clutter for PD and PFA computations by changing the intensity distribution into a gamma distribution. Multi-look processing is quite common for speckle reduction, with or without median filtering, and therefore merits some examination.

For multi-looking, the probability distributions of Equations 14 to 16 should be replaced with those below, when *n* is the number of looks [4]:

$$p(I) = \frac{n^n I^{n-1}}{(n-1)!\langle I\rangle^n} e^{\left(-\frac{nI}{\langle I\rangle}\right)}, \tag{24}$$

$$p(A) = \frac{2n^n A^{2n-1}}{(n-1)!\langle I\rangle^n} e^{\left(-\frac{nA^2}{\langle I\rangle}\right)}, \text{ and} \tag{25}$$

$$p(D) = \frac{n^n \ln 10}{10(n-1)!\langle I\rangle^n} e^{\left(\frac{nD\ln 10}{10} - \frac{ne^{\left(\frac{D\ln 10}{10}\right)}}{\langle I\rangle}\right)}. \tag{26}$$

The statistical values of the multi-looked and median-filtered image then approach the quantities in Table 3 for large N and n [4].

Table 3. Asymptotic Values of the Mean and Standard Deviation of a Multi-looked, Median-Filtered Homogeneous, Ideal Clutter Area for Large N and n

	Mean	Standard Deviation
Intensity	$\langle I\rangle$	$1.2\langle I\rangle/\sqrt{Nn}$
Amplitude	$\sqrt{\langle I\rangle}$	$0.6\sqrt{\langle I\rangle/Nn}$
Decibel Power (dB)	$10\log_{10}\langle I\rangle$	$5.4/\sqrt{Nn}$

Figure 11 shows sample results for the decibel domain shadow and clutter distribution with $n = 7$ multi-looking before and after median-filtering at 5 km range with all other parameters as before for comparison. Note the even greater Gaussian-like nature and larger separation between shadow and clutter distributions with multi-looking and median filtering. The PD and PFA results with multi-looking also shown in Figure 11 are consequently far better than without multi-looking. Median filtering in addition to multi-look image processing serves to enhance the PD and PFA performance even further, particularly at shorter ranges.

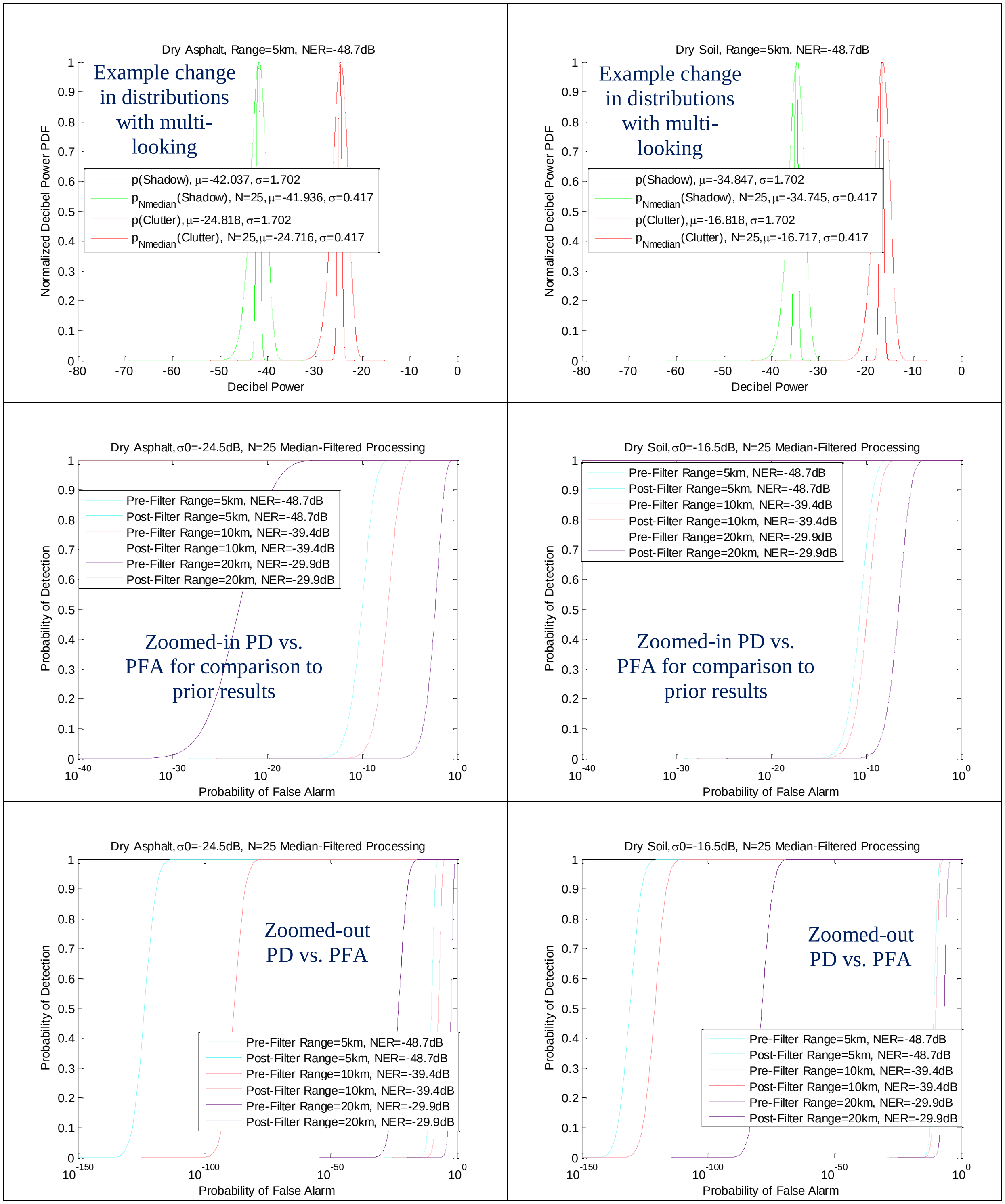

Figure 11. Before and After Effects of 5x5 Median Filtering for Asphalt and Soil versus Range of a Multi-looked (*n* = 7) Image

6. CONCLUSIONS

This report has presented median filtering effects on probability of detection and false alarm in SAR imagery for shadows in homogeneous, ideal clutter. Median filtering reduces speckle in imagery with some edge preservation at the expense of coarsened spatial resolution. Such non-linear post-processing effectively increases the shadow-to-clutter ratio of SAR imagery to increase detection and decrease false alarms by transforming the probability distributions of the target and interference into Gaussian-like distributions as a function of increasing window size. These statistical changes need to be considered when computing PD and PFA after median filtering, as well as the many system parameters of the platform, target, and scene which impact the clutter reflectivity and shadow noise such as range, platform velocity, grazing angle, clutter type, and the target mobility. We have shown that results assuming a stationary target under worst case platform and clutter conditions for an example SAR system perform no better than a probability of false alarm of about 10^{-15} for high probabilities of detection at the shortest (best case) ranges. We expect a moving target to perform no better than these results under similar conditions, since target mobility further blurs the shadow into the clutter during the synthetic aperture. Multi-looking may further enhance shadow detection PD and PFA in addition to median filtering.

"Detection is, or ought to be, an exact science, and should be treated in the same cold unemotional manner."

- Sir Arthur Conan Doyle

7. REFERENCES

1. M. A. Richards, *Fundamental of Radar Signal Processing*, McGraw-Hill, New York, 2005.

2. A. M. Raynal, D. L. Bickel, and A. W. Doerry, "Stationary and Moving Target Shadow Characteristics in Synthetic Aperture Radar," *Proceedings of the SPIE,* Defense, Security, and Sensing Symposium, Radar Sensor Technology Conference XVIII, Baltimore, MD, May 5-9, 2014.

3. D. L. Bickel, "Brief Note on Estimating Clutter Statistics," *Sandia National Laboratories Internal Memorandum*, Albuquerque, NM, September 30, 2011.

4. W. G. Rees and M. J. F. Satchell, "The effect of median filtering on synthetic aperture radar images," *International Journal of Remote Sensing*, vol. 18, no. 13, pp. 2887-2893, 1997.

5. J. F. Kenney and E. S. Keeping, *Mathematics of Statistics, 3rd Ed. Part 1 and 2*, D. Van Nostrand Company, Inc., Princeton, 1954.

6. T. Watkins, "The Probability Distribution of the Sample Median as a Function of Sample Size," *San Jose State University, Department of Economics,* http://www.sjsu.edu/faculty/watkins/samplemedian1.htm.

7. C. Oliver and S. Quegan, *Understanding Synthetic Aperture Radar Images*, SciTech Publishing, Inc., Raleigh, 2004.

8. A. W. Doerry, "Performance Limits for Synthetic Aperture Radar – Second Edition", *Sandia National Laboratories Report SAND2006-0821*, Albuquerque, NM, Feb. 2006.

9. W. G. Carrara, R. S. Goodman, and R. M. Majewski, *Spotlight Synthetic Aperture Radar: Signal Processing Algorithms*, Artech House, Boston, 1995.

10. F. T. Ulaby and M. C. Dobson, *Radar Scattering Statistics for Terrain,* Artech House, Inc., Norwood, MA, 1989.

DISTRIBUTION

1	John Miller General Atomics ASI, MS 16868 Via Del Campo Ct San Diego, CA 92127		(electronic copy)
1	Edward Bishop General Atomics ASI, MS 16761 Via Del Campo Ct San Diego, CA 92127		(electronic copy)
1	Volker Horndt General Atomics ASI, MS 16761 Via Del Campo Ct San Diego, CA 92127		(electronic copy)

Further distribution to General Atomics employees is authorized.

1	MS0509	K. D. Meeks	5300	(electronic copy)
1	MS0519	A. M. Raynal	5344	
1	MS0519	J. A. Ruffner	5349	
1	MS0519	L. M. Klein	5349	
1	MS0519	A. W. Doerry	5349	
1	MS0532	J. J. Hudgens	5340	
1	MS0532	B. L. Burns	5340	(electronic copy)
1	MS0532	W. H. Hensley	5344	(electronic copy)
1	MS0899	Technical Library	9536	(electronic copy)

“There are more things to alarm us that to harm us, and we suffer more often in apprehension than reality.”

- Lucius Annaeus Seneca